

Synthesis Design | Hot Paper |

Tiffany M. Smith Pellizzeri,^[a, b] Colin D. McMillen,^[a] and Joseph W. Kolis*^[a]

Abstract: Materials with triangular arrangements of transition metal ions are of great interest for their complex magnetism resulting from geometric frustration. This paper describes the stepwise formation of kagome lattices of open shell transition-metal ions from half-delta chains to delta/sawtooth chains, and finally kagome nets. The systems can be viewed as a testbed for magnetic studies since a variety of spin states can be introduced across the same structure type, and progress through increasing levels of structural complexity and dimensionality. The synthetic and structural development of this continuum is studied here in well-formed single crystals of $A_2M_3(\text{MoO}_4)_3(\text{OH})_2$ ($A = \text{K, Rb}$; $M = \text{Mn, Co}$), $\text{Cs}M_2(\text{MoO}_4)_2(\text{OH})$ ($M = \text{Mn, Fe, Co, Zn}$), and $\text{KM}_3(\text{MoO}_4)_2\text{O}(\text{OH})$ ($M = \text{Mn}$).

The synthesis and structural characterization of materials with open-shell transition metals in geometrically frustrated lattices are critical to the study of complex magnetic behavior.^[1–5] Magnetic frustration is an essential component of quantum spin liquids and other quantum materials. Numerous structural topologies can induce geometric frustration, including 3D frameworks with trigonal symmetry (e.g. perovskite or pyrochlore), or lower-dimensional honeycomb, kagome, ladder, strip, or chain arrangements, among others.^[6–10] It is of interest to develop synthetic approaches to target specific compositions of such structures for magnetic studies. The synthesis of pyrochlores^[11,12] and jarosites^[1] provide good examples of this approach. It is particularly important to develop rational synthetic pathways to examples of new magnetically frustrated materials. A rational approach to new low-dimensional solids with triangular lattices is desirable, particularly one that enables the variation of spin states.

Tetrahedral oxyanions are excellent building blocks with open-shell, first row transition-metal ions to form a variety of

low-dimensional structures.^[13] The tetrahedral building blocks also contain trigonal symmetry that can lead to geometric frustration. Vanadate oxyanions, $(\text{VO}_4)^{3-}$, are particularly versatile building blocks for complex magnetic structures containing divalent and trivalent transition metals.^[14–18] The presence of empty d-orbitals in the oxyanion bridging units can also have a significant effect on the value and sign of the coupling constant. With its similar size, tetrahedral structure, and empty d-orbitals, the molybdate oxyanion, $(\text{MoO}_4)^{2-}$, can be expected to adopt many of the same structural roles as $(\text{VO}_4)^{3-}$. The crystal chemical substitutions of additional constituent elements (e.g. alkali and alkaline earth metal ions that have no effect on the magnetic properties) provide an additional degree of freedom in the formation of new phases.


In the present study, we examine a series of synthetically and structurally related alkali transition-metal molybdates that demonstrate a stepwise approach to magnetically frustrated systems, including the prototype kagome lattice. Three classes of compounds were prepared from high temperature (580 °C) and high pressure (130–180 MPa) hydrothermal fluids: $A_2M_3(\text{MoO}_4)_3(\text{OH})_2$ ($A = \text{K, Rb}$; $M = \text{Mn, Co}$), $\text{Cs}M_2(\text{MoO}_4)_2(\text{OH})$ ($M = \text{Mn, Fe, Co, Zn}$), and $\text{KM}_3(\text{MoO}_4)_2\text{O}(\text{OH})$ ($M = \text{Mn}$).^[19–22] Specific synthetic procedures are provided in the Supporting Information. These compounds all contain edge-shared transition-metal octahedra that demonstrate the stepwise construction of triangular arrangements of increasing complexity and dimensionality to ultimately form an ideal kagome layer (Figure 1).

The transition-metal ions in $A_2M_3(\text{MoO}_4)_3(\text{OH})_2$ ($A = \text{K, Rb}$; $M = \text{Mn, Co}$) form a half-delta chain (Figure 1a, 2a). In this arrangement, octahedral metal ions condense into triangular clusters by edge sharing of the $[\text{MO}_6]$ octahedra. These triangular clusters can be further elaborated into the full-delta, or sawtooth chain as exemplified by $\text{Cs}M_2(\text{MoO}_4)_2(\text{OH})$ ($M = \text{Mn, Fe, Co, Zn}$) (Figure 1b, 2b). In this more complex chain, transition-metal triangles condense across both sides of a central axis. In this way, the triangular clusters share transition-metal corners directly as the chain propagates. The condensation of delta chains continues with one another through the apices of the triangular clusters resulting in the ultimate formation of the kagome layers found in $\text{KM}_3(\text{MoO}_4)_2\text{O}(\text{OH})$ ($M = \text{Mn}$) (Figure 1c, 2c). Here, all the transition metal corners are shared by neighboring clusters.

Structural features pertaining to the various triangular magnetic lattices are summarized in Table 1. Complete data from the crystallographic refinements are provided in the Supporting Information. The metal–oxygen distances are consistent

[a] Dr. T. M. Smith Pellizzeri, Dr. C. D. McMillen, Prof. J. W. Kolis
Department of Chemistry, Clemson University
Clemson, SC 29634 (USA)
E-mail: kjoseph@clemson.edu

[b] Dr. T. M. Smith Pellizzeri
Department of Chemistry and Biochemistry
Eastern Illinois University, Charleston, IL 61920 (USA)

 Supporting information and the ORCID identification number(s) for the author(s) of this article can be found under:
<https://doi.org/10.1002/chem.201904193>

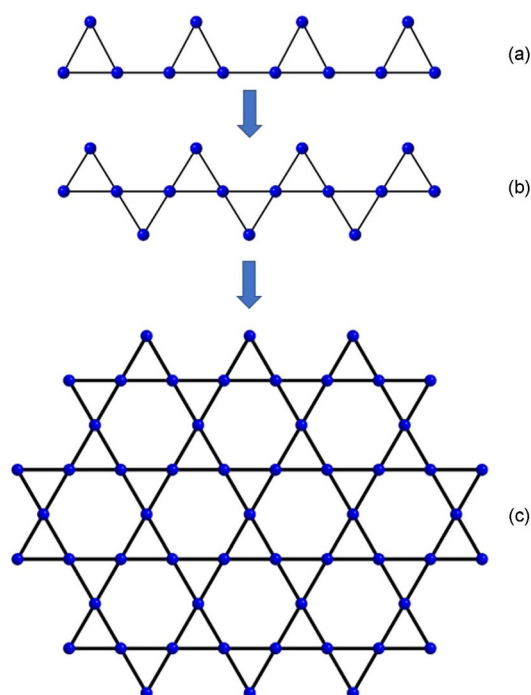


Figure 1. Schematic representation of the triangular lattice progression of the half-delta chain of $A_2M_3(\text{MoO}_4)_3(\text{OH})_2$ (a) to the delta chain of $\text{Cs}M_2(\text{MoO}_4)_2(\text{OH})$ (b) to the kagome layer of $\text{KM}_3(\text{MoO}_4)_2\text{O}(\text{OH})$ (c). Blue spheres represent transition metals, with black lines representing edge-shared interactions through oxygen atoms of the $[\text{MO}_6]$ octahedra.

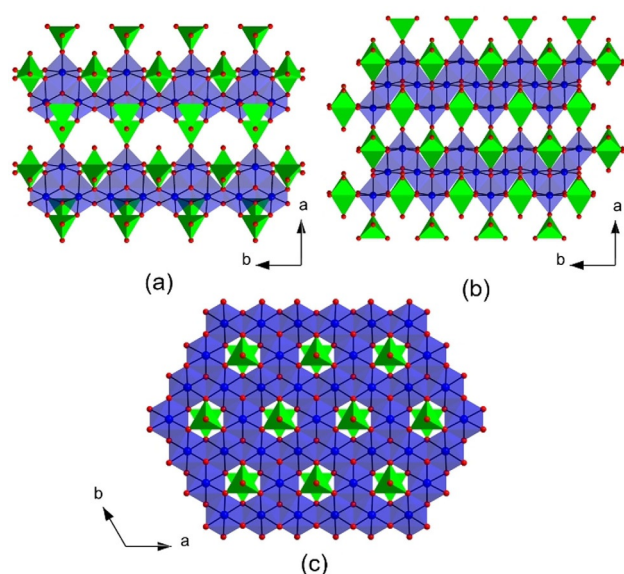


Figure 2. Transition-metal molybdate motifs in $A_2M_3(\text{MoO}_4)_3(\text{OH})_2$ (a), $\text{Cs}M_2(\text{MoO}_4)_2(\text{OH})$ (b), and $\text{KM}_3(\text{MoO}_4)_2\text{O}(\text{OH})$ (c). Blue spheres and polyhedra represent transition metals, green polyhedra are molybdenum, and red spheres are oxygen.

with those of high-spin electronic configurations. The triangular units in the half-delta chains of $A_2M_3(\text{MoO}_4)_3(\text{OH})_2$ and the delta chains of $\text{Cs}M_2(\text{MoO}_4)_2(\text{OH})$ contain two crystallographically distinct transition-metal sites forming isosceles triangles through the shared edges of the octahedra. In the case of the

Table 1. Summary of transition-metal (<i>M</i>) molybdates in the present study.			
Compound	M–O distance [Å]	M–M distances [Å]	Triangular lattice
$\text{K}_2\text{Mn}_3(\text{MoO}_4)_3(\text{OH})_2$	2.200(3)	3.3688(7) (×2) 3.1656(8) 3.0818(8) ^[a]	half-delta chain
$\text{K}_2\text{Co}_3(\text{MoO}_4)_3(\text{OH})_2$	2.115(3)	3.2268(7) (×2) 3.0673(8) 3.0162(8) ^[a]	half-delta chain
$\text{Rb}_2\text{Mn}_3(\text{MoO}_4)_3(\text{OH})_2$	2.196(4)	3.3748(10) (×2) 3.1687(14) 3.1068(14) ^[a]	half-delta chain
$\text{CsMn}_2(\text{MoO}_4)_2(\text{OH})$	2.186(3)	3.2685(5) (×2) 3.0948(1) (×2)	delta chain
$\text{CsFe}_2(\text{MoO}_4)_2(\text{OH})$	2.138(4)	3.1906(6) (×2) 3.0552(1) (×2)	delta chain
$\text{CsCo}_2(\text{MoO}_4)_2(\text{OH})$	2.103(3)	3.1280(4) (×2) 3.0206(1) (×2)	delta chain
$\text{CsZn}_2(\text{MoO}_4)_2(\text{OH})$	2.116(4)	3.1600(5) (×2) 3.0383(1) (×2)	delta chain
$\text{KMn}_3(\text{MoO}_4)_2\text{O}(\text{OH})$	2.153(4)	3.0512(2) (×4)	kagome layer

[a] Mn–Mn bridging distance between triangular clusters in the chain.

delta chain, an additional MO_6 group bridges the triangles on the opposite side embellishing the chains. Finally, the kagome layers of $\text{KM}_3(\text{MoO}_4)_2\text{O}(\text{OH})$ are formed from equilateral triangles containing only one unique transition metal, making that system an example of an ideal kagome layer. All three structure types possess distorted $[\text{MO}_6]$ octahedra, with *M*–O bond lengths occurring over a wide range.

It is important to understand the role of the molybdate tetrahedra in the overall structures. These can act both as structural bridging units and as a magnetic coupling pathway in the same way as sulfates do in jarosites for example.^[1] In the case of the half-delta chains of $A_2M_3(\text{MoO}_4)_3(\text{OH})_2$ the chain propagates along the *b*-axis, and is decorated by three unique $[\text{MoO}_4]$ tetrahedra. Two $[\text{MoO}_4]$ units act as corner sharing bridges to neighboring chains to form a layered substructure (Figure 2a) ultimately creating a three-dimensional framework (Figure 3a). Two oxygen atoms of one chain are connected to one oxygen atom of a neighboring chain through the molybdenum atom. The third unique molybdate group sits in a pocket of the chain, bonding to three oxygen atoms on one chain, but not bridging between chains. The delta chains of $\text{Cs}M_2(\text{MoO}_4)_2(\text{OH})$ also propagate along the *b*-axis, flanked by two unique $[\text{MoO}_4]$ tetrahedra. One links two chains through two oxygen atoms of one chain to one oxygen atom of the neighboring chain creating a two-dimensional transition-metal molybdate layer (Figure 2b, 3b). The second molybdate group sits in a pocket of the delta chain in the same way that is observed in the half-delta chain. In $\text{KM}_3(\text{MoO}_4)_2\text{O}(\text{OH})$ there is only one unique $[\text{MoO}_4]$ group that is aligned with the hexagonal voids of the kagome layer. In this way, molybdate groups terminate the top and bottom of these layers, with crystallographic three-fold symmetry along the *c*-axis (Figure 2c, 3c). This is a particularly useful example of how the inherent three-fold symmetry of tetrahedral building blocks can be used to

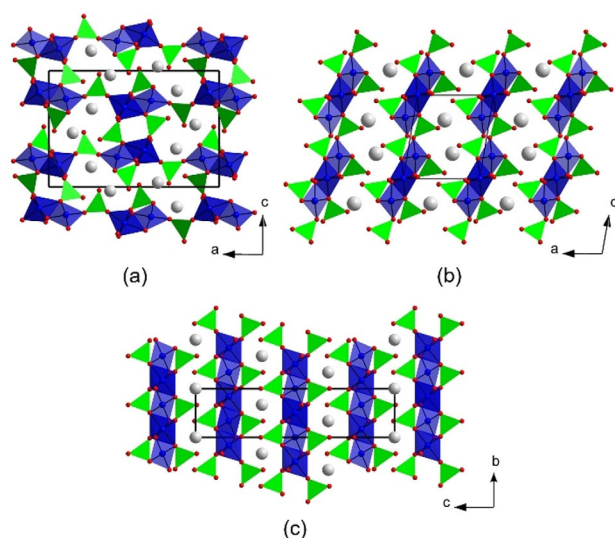


Figure 3. Extended structures of triangular lattice materials viewed along the direction of chain propagation in $A_2M_3(\text{MoO}_4)_3(\text{OH})_2$ (a) and $\text{CsM}_2(\text{MoO}_4)_2(\text{OH})$ (b), and along the length of the kagome layers in $\text{KM}_3(\text{MoO}_4)_2\text{O}(\text{OH})$ (c). Color scheme is the same as in Figure 2, with alkali metal atoms shown as silver spheres.

template triangular relationships in materials. In all of these structures, each molybdate group bridges to transition-metal ions through three oxygen atoms while the fourth oxygen atom on all the $[\text{MoO}_4]$ units exhibits the shortest Mo–O bond lengths, and bonds to the alkali metals located in the framework voids or between the transition-metal molybdate sheets (Figure 3).

The $A_2M_3(\text{MoO}_4)_3(\text{OH})_2$ and $\text{CsM}_2(\text{MoO}_4)_2(\text{OH})$ systems represent two new structure types with rare triangular chains for magnetic study. The $\text{KM}_3(\text{MoO}_4)_2\text{O}(\text{OH})$ system is an interesting modification of the vesignieite ($\text{BaCu}_3(\text{VO}_4)_2(\text{OH})_2$) archetype containing vanadate building blocks and well known to exhibit complex magnetic properties and structural subtleties.^[23–29] Molybdates of this type were previously found for the later divalent transition metals as $(\text{NH}_4)\text{HM}_2(\text{MoO}_4)_2(\text{OH})_2$ ($M = \text{Co-Zn}$), but in these cases, the transition-metal site is 2/3 occupied.^[30–33] This partial occupancy would complicate the desired spin frustration behavior. The present study of $\text{KMn}_3(\text{MoO}_4)_2\text{O}(\text{OH})$ is to our knowledge, the first report of a vesignieite-type compound based on Mn^{2+} , and has full occupancy at the transition metal site. This makes it one of the relatively few examples of an ideal kagome symmetry for a high magnetic spin ($S = 5/2$) metal ion.^[34] In all cases, the presence of structural hydroxide was confirmed by IR spectroscopy, and the hydrogen atoms were located from the difference electron density maps and refined satisfactorily in these positions. Given the structural connectivity already enabled by the bridging oxides in the transition-metal molybdate motifs, the primary role of the hydroxide groups is to ensure charge neutrality.

The hydrothermal fluids used here resemble natural alkali brines that can participate in the chemical reactions or serve as mineralizers to facilitate reactivity and crystal growth. Products are controlled by the ratio of reactants and the nature of

the mineralizer. For example, a 1:1 mole ratio reaction of MnO and MoO_3 produced $\text{K}_2\text{Mn}_3(\text{MoO}_4)_3(\text{OH})_2$ when using K_2CO_3 as a mineralizer, and $\text{CsMn}_2(\text{MoO}_4)_2(\text{OH})$ when using Cs_2CO_3 as a mineralizer. In contrast, the same 1:1 reaction of MnO and MoO_3 by using a KOH/KCl mineralizer produced $\text{KMn}_3(\text{MoO}_4)_2\text{O}(\text{OH})$. The ability to introduce alkali metals of different sizes, and the use of different mineralizers to influence the resulting phase formation is an important factor in developing designed syntheses such as these. Simple variation of the chemistry leads to straightforward condensation of chains. This approach enabled the synthesis of compounds containing several different divalent transition metal ions, allowing the comparison of the magnetic properties of significantly different spin states ($S = 5/2$ for Mn^{2+} , $S = 2$ for Fe^{2+} , $S = 3/2$ for Co^{2+}) for a given structure type. This series of compounds, featuring a continuum of triangular lattices that can be condensed in a stepwise fashion, also enables magnetic studies of kagome lattices and component lattices with high spin value transition metals. The precision synthesis forms the groundwork for detailed magnetic neutron diffraction investigations that are underway.

Acknowledgements

We are indebted to the NSF DMR-1808371 for support of this work.

Conflict of interest

The authors declare no conflict of interest.

Keywords: geometric frustration • hydrothermal synthesis • molybdenum • transition metals • triangular lattice

- [1] D. G. Nocera, B. M. Bartlett, D. Grohol, D. Papoutsakis, M. P. Shores, *Chem. Eur. J.* **2004**, *10*, 3850–3859.
- [2] J. Greedan, *J. Mater. Chem.* **2001**, *11*, 37–53.
- [3] A. P. Ramirez, *Ann. Rev. Mater. Sci.* **1994**, *24*, 453–480.
- [4] A. P. Ramirez, A. Hayashi, R. J. Cava, R. Siddharthan, B. S. Shastry, *Nature* **1999**, *399*, 333–335.
- [5] P. Mendels, F. Bert, *C. R. Phys.* **2016**, *17*, 455–470.
- [6] A. Harrison, *J. Phys. Condens. Matter* **2004**, *16*, S553–S572.
- [7] S. K. Pati, C. N. R. Rao, *Chem. Commun.* **2008**, 4683–4693.
- [8] H. Kikuchi, Y. Fujii, D. Takahashi, M. Azuma, Y. Shimakawa, T. Taniguchi, A. Matsuo, K. Kindo, *J. Phys. Conf. Ser.* **2011**, *320*, 012045.
- [9] R.-S. Chang, S.-L. Wang, K.-H. Li, *Inorg. Chem.* **1997**, *36*, 3410–3413.
- [10] V. O. Garlea, L. D. Sanjeewa, M. A. McGuire, P. Kumar, D. Sulejmanovic, J. He, S.-J. Hwu, *Phys. Rev. B* **2014**, *89*, 014426.
- [11] B. A. Trump, S. M. Koohpayeh, K. J. T. Livi, J.-J. Wen, K. E. Arpino, Q. M. Ramasse, R. Brydson, M. Feygenson, H. Takeda, M. Takigawa, K. Kimura, S. Nakatsujii, C. L. Broholm, T. M. McQueen, *Nat. Commun.* **2018**, *9*, 1–10.
- [12] M. Powell, L. D. Sanjeewa, C. D. McMillen, K. A. Ross, C. L. Sarkis, J. W. Kolis, *Cryst. Growth Des.* **2019**, *19*, 4920–4926.
- [13] C. D. McMillen, J. W. Kolis, *Dalton Trans.* **2016**, *45*, 2772–2784.
- [14] L. D. Sanjeewa, M. A. McGuire, V. O. Garlea, L. Hu, G. Chumanov, C. D. McMillen, J. W. Kolis, *Inorg. Chem.* **2015**, *54*, 7014–7020.
- [15] L. D. Sanjeewa, M. A. McGuire, C. D. McMillen, D. Willett, G. Chumanov, J. W. Kolis, *Inorg. Chem.* **2016**, *55*, 9240–9249.
- [16] L. D. Sanjeewa, M. A. McGuire, T. M. Smith Pellizzeri, C. D. McMillen, V. O. Garlea, D. Willett, G. Chumanov, J. W. Kolis, *J. Solid State Chem.* **2016**, *247*, 30–37.

- [17] L. D. Sanjeeva, V. O. Garlea, M. A. McGuire, M. Frontzek, C. D. McMillen, K. Fulle, J. W. Kolis, *Inorg. Chem.* **2017**, *56*, 14842–14849.
- [18] L. D. Sanjeeva, V. O. Garlea, M. A. McGuire, C. D. McMillen, J. W. Kolis, *Inorg. Chem.* **2019**, *58*, 2813–2821.
- [19] Representative crystallographic data: $\text{K}_2\text{Mn}_3(\text{MoO}_4)_3(\text{OH})_2$: space group *Pnma*; $a = 18.3294(6)$, $b = 6.2474(2)$, $c = 12.4969(4)$ Å; $V = 1431.03(8)$ Å³; $Z = 4$; $D = 3.513$; 11174 reflections (1601 unique); $R1 = 0.0202$, $wR2 = 0.0455$.
- [20] Representative crystallographic data: $\text{CsMn}_2(\text{MoO}_4)_2(\text{OH})$: space group *P2₁/m*; $a = 8.3056(4)$, $b = 6.1896(2)$, $c = 9.3361(4)$ Å; $\beta = 99.862(2)^\circ$; $V = 472.86(3)$ Å³; $Z = 2$; $D = 4.071$; 19081 reflections (1065 unique); $R1 = 0.0149$, $wR2 = 0.0393$.
- [21] Representative crystallographic data: $\text{KMn}_3(\text{MoO}_4)_2\text{O}(\text{OH})$: space group *R-3m*; $a = 6.1024(3)$, $c = 21.5384(11)$ Å; $V = 694.62(8)$ Å³; $Z = 3$; $D = 3.993$; 2606 reflections (207 unique); $R1 = 0.0302$, $wR2 = 0.0811$.
- [22] CCDC 1951535, 1951536, 1951537, 1951538, 1951539, 1951540, 1951541 and 1951542 contain the supplementary crystallographic data for this paper. These data are provided free of charge by The Cambridge Crystallographic Data Centre.
- [23] D. Boldrin, B. Fåk, E. Canévet, J. Ollivier, H. C. Walker, P. Manuel, D. D. Khalyavin, A. S. Wills, *Phys. Rev. Lett.* **2018**, *121*, 107203.
- [24] D. Boldrin, K. Knight, A. S. Wills, *J. Mater. Chem. C* **2016**, *4*, 10315–10322.
- [25] D. Boldrin, A. S. Wills, *J. Mater. Chem. C* **2015**, *3*, 4308–4315.
- [26] D. Freedman, R. Chisnell, T. M. McQueen, Y. S. Lee, C. Payen, D. G. Nocera, *Chem. Commun.* **2012**, *48*, 64–66.
- [27] H. Yoshida, Y. Michiue, E. Takayama-Muromachi, M. Isobe, *J. Mater. Chem.* **2012**, *22*, 18793–18796.
- [28] M. Zhesheng, H. Ruilin, Z. Xiaoling, *Acta Geol. Sin.* **1991**, *4*, 145–151.
- [29] T. Đorđević, L. Karanović, *Acta Crystallogr., Sect. C: Struct. Chem.* **2013**, *69*, 114–118.
- [30] H. Pezerat, *Bull. Soc. Fr. Mineral. Cristallogr.* **1967**, *90*, 549–557.
- [31] D. Levin, S. L. Soled, J. Y. Ying, *Chem. Mater.* **1996**, *8*, 836–843.
- [32] D. Levin, S. L. Soled, J. Y. Ying, *Inorg. Chem.* **1996**, *35*, 4191–4197.
- [33] C.-D. Wu, C.-Z. Lu, X. Lin, S.-F. Lu, H.-H. Zhuang, J.-S. Huang, *J. Alloys Compd.* **2004**, *368*, 342–348.
- [34] D. Grohol, D. G. Nocera, D. Papoutsakis, *Phys. Rev. B* **2003**, *67*, 064401.

 Manuscript received: September 11, 2019

Accepted manuscript online: September 27, 2019

Version of record online: November 7, 2019